Journal of Theoretical and Applied Vibration and Acoustics 1(2) 73-84 (2015)

I S A V

Journal of Theoretical and Applied Vibration and Acoustics

journal homepage: http://tava.isav.ir

Nonlinear energy harvesting through a multimodal electro-mechanical system

Moein Mohammadpour, Morteza Dardel *, Mohammad Hasan Ghasemi, Mohammad Hadi Pashaei

Department of Mechanical Engineering, Babol Noshirvani University of Technology, Postal Code: 47148-71167, Shariati Street, Babol, Mazandaran, Iran

KEYWORDS

Nonlinear energy harvesting

Multimodal duffing oscillator

Complexification averaging method

Arc length continuation method

ABSTRACT

A semi-analytical method is used to illustrate the behavior of a multimodal nonlinear electromechanical system which is under base-excitation. System is considered as piezo-ceramic patches attached to a cantilever beam coupled to a resistive load. The cantilever beam is modeled as a nonlinear Timoshenko beam using Assumed Mode method and equations of motion are derived through Lagrange's equation. Nonlinear multimodal equations are solved with Complexification Averaging method and results are compared with numerical simulations. Arc length Continuation method is used to achieve frequency response of the system. Results are presented for different values of geometric and physical parameters and the effect of this variations are discussed.

1. Introduction

Energy harvesting form ambient vibrations has been most heavily researched in the last decade because of its useful applications [1]. One of this applications is preparing the energy requested by small electronics like wireless sensors that are hard to reach and replacement of their battery is impossible. Although linear energy harvesters were proposed at first, later research indicated that the narrow band nature of these systems affects their efficiency [2]. Nonlinear energy harvesting systems are proposed as a solution to this problem [3].

Mann and Sims [4] introduced an energy harvester which utilizes magnetic levitation in order to produce a system with a tenable resonance. The results indicated that response of the nonlinear system is in the large amplitude oscillations in wider range of frequencies relatively. In [5, 6], a Duffing oscillator for broadband piezoelectric energy harvesting is investigated experimentally and analytically. They used a cantilever piezoelectric beam as a nonlinear energy harvester. It is showed that, there is a region in which the system has three possible responses and there is jump

* Corresponding Author: Morteza Dardel, Email: dardel@nit.ac.ir

phenomenon in the frequency response capture of the system. It is showed that, the nonlinear system has broader frequency bandwidth over the linear one. In [7], Karami and Inman proposed a method to approximate electromechanical coupling as equivalent changes in damping and excitation frequency in order to simplify the analyses of energy harvesting systems. The method in this paper is verified by hybrid piezoelectric and electromagnetic energy harvester system in linear, softly nonlinear and bi-stable cases. They showed when an optimal resistant load is used, the amplitude of mechanical vibrations is the smallest.

Some of researchers considered random excitations in order to examine the performance of the nonlinear energy harvesters. Daqaq [8] investigated energy harvesting of a unit-modal Duffing oscillator under white and color Gaussian noise and concluded that the mean output power of the harvester is not influenced by the stiffness-type nonlinearities, however other types of nonlinearities such as damping and inertia may be beneficial. Authors of [9] studied energy harvesting of monostable Duffing oscillator under Gaussian excitation. They examined the effects of spectral density of random excitation and the cubic nonlinearity on the output voltage. The results indicated that increases in the cubic nonlinearity led to increase in output voltage for reasonable larger excitation spectral density. However, for smaller density, output voltage slightly decreases with the increase in cubic nonlinearity. Masan and Daqaq in [10] investigated the influence of stiffness-type nonlinearity on the transduction of vibratory energy harvesters under band-limited noise. They considered the harvester as a bimorph clamped-clamped beam subjected to an axial load so as to analyse both pre-buckling and post-buckling configurations. The results pointed out that for small base accelerations both configurations produce maximum voltage when the centre of frequency of the excitation matches the tuned oscillation frequency of the harvester, regardless to the frequency bandwidth which means that the nonlinearity can be neglected in this case. Nevertheless, in larger excitation amplitudes maximum voltage variance will occur at larger or smaller frequencies due to different nature of nonlinearity (hardening or softening) in both configurations.

In most former studies, energy harvesting systems are considered as uni-modal systems, however, a single-mode approximation underestimates the actual output power of the device [3] at the other hand multimodal systems' responses are in the larger amplitudes in a wider range of frequency over their single-mode counterparts. In this paper, an assumed-mode modelling of the bimorph piezoelectric energy harvester is presented and the effect of the number of the shape modes is investigated. The beam is modelled using Timoshenko beam theory and equations of motion derived using Lagrange's equation. In multimodal nonlinear case applying perturbation techniques is very complicated because there are lots of resonance frequencies that should be investigated separately and for higher number of modes it is impossible to use perturbation techniques. Because of this, nonlinear multimodal equations of motion is solved using Complexification Averaging Method. Frequency response captures are obtained through Arc Length Continuation Method. Effect of changing the number of shape modes, base acceleration, and piezoelectric patches' length are given.

2. Assumed-mode modeling of piezoelectric energy harvester

2.1. Bimorph piezoelectric energy harvester and modeling assumptions

Two piezoelectric patches are coupled to the upper and lower faces of the beam structure and perfectly conductive electrodes fully cover the piezoelectric patches and the electrodes are coupled to a resistive electrical load in a series configuration (Fig. 1). A tip mass is attached to cantilever con-figuration. The system is under base excitation and the base motion can be expressed as:

$$w_b(t) = g(t) \tag{1}$$

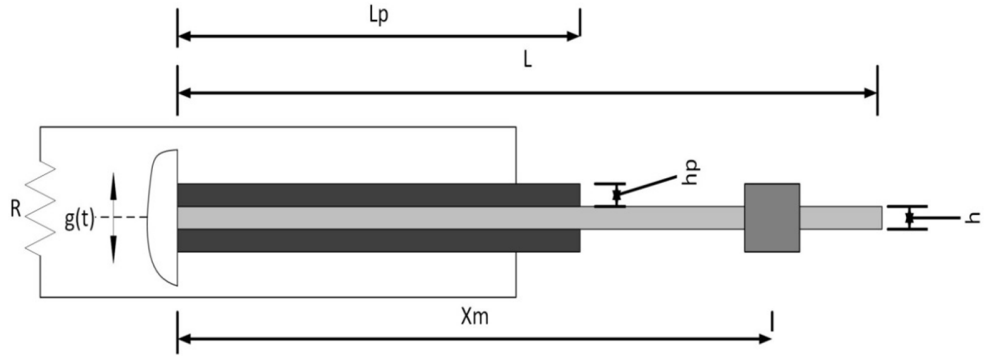

Fig. 1. Piezoelectric energy harvester configuration

The longitudinal axis is denoted by x_1 and the transverse axis by x_3.

2.2. Displacement field and energy terms

The displacement field in Timoshenko model is [3]:

$$u_1 = -x_3\Phi(x_1,t), \qquad u_2 = 0, \qquad u_3 = u_3(x_1,t) \tag{2}$$

where u_1, u_3 are the displacements in longitudinal and transverse directions and $\Phi(x_1,t)$ is the cross section rotation. The nonlinear strains are:

$$S_1 = \frac{\partial u_1}{\partial x_1} + \frac{1}{2}\left[\left(\frac{\partial u_1}{\partial x_1}\right)^2 + \left(\frac{\partial u_2}{\partial x_1}\right)^2 + \left(\frac{\partial u_3}{\partial x_1}\right)^2\right] = -x_3\frac{\partial \Phi}{\partial x_1} + \frac{1}{2}\left(\frac{\partial u_3}{\partial x_1}\right)^2 \tag{3}$$

$$S_5 = \frac{\partial u_1}{\partial x_3} + \frac{\partial u_3}{\partial x_1} = \frac{\partial u_3}{\partial x_1} - \Phi \tag{4}$$

The substructure beam stresses are:

$$T_1^b = ES_1 = -Ex_3\frac{\partial \Phi}{\partial x_1} + \frac{1}{2}E\left(\frac{\partial u_3}{\partial x_1}\right)^2 \tag{5}$$

$$T_5^b = \kappa G_b S_5 = \kappa G_b\left(\frac{\partial u_3}{\partial x_1} - \Phi\right) \tag{6}$$

where E and G_b are the elastic and shear modulus of the beam substructure. Stresses in piezoelectric layers are:

$$T_{1_1}^p = c_{11}^\epsilon S_1 - e_{31}\epsilon_3 = -\mathrm{c}_{11}^\epsilon x_3 \frac{\partial \Phi}{\partial x_1} + \frac{\mathrm{c}_{11}^\epsilon}{2}\left(\frac{\partial u_3}{\partial x_1}\right)^2 + e_{31}\frac{v}{h_p} \tag{7}$$

$$T_{1_2}^p = c_{11}^\epsilon S_1 - e_{31}\epsilon_3 = -\mathrm{c}_{11}^\epsilon x_3 \frac{\partial \Phi}{\partial x_1} + \frac{\mathrm{c}_{11}^\epsilon}{2}\left(\frac{\partial u_3}{\partial x_1}\right)^2 - e_{31}\frac{v}{h_p} \tag{8}$$

$$T_{5_{1,2}}^p = \kappa c_{55}^\epsilon \left(\frac{\partial u_3}{\partial x_1} - \Phi\right) \tag{9}$$

where c_{55}^ϵ and e_{31} are the shear modulus and effective piezoelectric stress constant of piezoelectric layers. According to equations (3-10), the total potential is:

$$U = \frac{1}{2}\iiint_{V_b} \underline{S}^t \underline{T}^b \, dV_b + \frac{1}{2}\iiint_{V_{p_1}} \underline{S}^t \underline{T}^p \, dV_{p_1} + \frac{1}{2}\iiint_{V_{p_2}} \underline{S}^t \underline{T}^p \, dV_{p_2}$$

$$= \frac{1}{2}\int_0^L \left\{ E\left(I_b\left(\frac{\partial \Phi}{\partial x_1}\right)^2 + \frac{1}{4}A_b\left(\frac{\partial u_3}{\partial x_1}\right)^4\right) + \kappa G_b A_b\left(\left(\frac{\partial u_3}{\partial x_1}\right)^2 + \Phi^2 - 2\frac{\partial u_3}{\partial x_1}\Phi\right)\right\} dx_1 \tag{10}$$

$$+ \int_0^{L_1} \left\{ c_{11}^\epsilon\left(I_p\left(\frac{\partial \Phi}{\partial x_1}\right)^2 + \frac{1}{4}A_p\left(\frac{\partial u_3}{\partial x_1}\right)^4\right) - e_{31}Q_p\frac{v}{h_p}\frac{\partial \Phi}{\partial x_1} + \kappa c_{55}^\epsilon A_p\left(\left(\frac{\partial u_3}{\partial x_1}\right)^2 + \Phi^2 - 2\frac{\partial u_3}{\partial x_1}\Phi\right)\right\} dx_1$$

where I_b, A_b, I_p, A_p and Q_p are the second moment of area and cross section area of the substructure beam, the second moment of area, the cross section area and first moment of area of piezoelectric layer. Electrical load displacement in piezoelectric layers are [3]:

$$D_{3_1} = e_{31}S_1 + \xi_{33}^S\epsilon_3 = -e_{31}x_3\frac{\partial \Phi}{\partial x_1} + \frac{e_{31}}{2}\left(\frac{\partial u_3}{\partial x_1}\right)^2 - \xi_{33}^S\frac{v}{h_p} \tag{11}$$

$$D_{3_2} = e_{31}S_1 + \xi_{33}^S\epsilon_3 = -e_{31}x_3\frac{\partial \Phi}{\partial x_1} + \frac{e_{31}}{2}\left(\frac{\partial u_3}{\partial x_1}\right)^2 + \xi_{33}^S\frac{v}{h_p} \tag{12}$$

where ξ_{33}^S is the permittivity of piezoelectric layer. The work of electric field in piezoelectric layers is:

$$W_e = \frac{1}{2}\iiint_{V_{p_1}} \underline{\epsilon}^t \underline{D} \, dV_{p_1} + \frac{1}{2}\iiint_{V_{p_2}} \underline{\epsilon}^t \underline{D} \, dV_{p_2} = e_{31}Q_p\int_0^{L_1}\frac{v}{h_p}\frac{\partial \Phi}{\partial x_1}dx_1 + \xi_{33}^S A_e\frac{v^2}{h_p} \tag{13}$$

The total displacement is:

$$\tilde{u}(x_1, t) = \{-x_3\Phi \quad 0 \quad u_3\}^t + \{0 \quad 0 \quad w_b\}^t \tag{14}$$

The total kinetic energy according to (14) is:

$$T = \frac{1}{2}\left(\iiint_{V_b} \rho_b \left(\left(-x_3\frac{\partial\Phi}{\partial t}\right)^2 + \left(\frac{\partial u_3}{\partial t} + \frac{\partial w_b}{\partial t}\right)^2\right) dV_b + 2\iiint_{V_p} \rho_p \left(\left(-x_3\frac{\partial\Phi}{\partial t}\right)^2 + \left(\frac{\partial u_3}{\partial t} + \frac{\partial w_b}{\partial t}\right)^2\right) dV_p\right)$$
$$\frac{1}{2}\left(\int_0^L \rho_b \left(I_b\left(\frac{\partial\Phi}{\partial t}\right)^2 + A_b\left(\left(\frac{\partial u_3}{\partial t}\right)^2 + \dot{g}^2 + 2\frac{\partial u_3}{\partial t}\dot{g}\right)\right) dx_1 \right. \tag{15}$$
$$\left. + 2\int_0^{L_1} \rho_p \left(I_p\left(\frac{\partial\Phi}{\partial t}\right)^2 + A_p\left(\left(\frac{\partial u_3}{\partial t}\right)^2 + \dot{g}^2 + 2\frac{\partial u_3}{\partial t}\dot{g}\right)\right) dx_1\right)$$

The Rayleigh dissipation function for external damping is:

$$D = \frac{1}{2}c\left(\frac{\partial u_3}{\partial t}\delta(x_d)\right)^2 \tag{16}$$

where c is the damping coefficient. The non-conservative work in electric resistive load is:

$$W_{nc} = 2Qv \tag{17}$$

where Q and v are the electrical load crossing resistance and voltage of each piezoelectric layer

2.3. Assumed-mode method

For Timoshenko beam first we define new parameter as:

$$\beta = \frac{\partial u_3}{\partial x_1} - \Phi \tag{18}$$

Allowable test functions must satisfy natural and geometric boundary conditions. Displacements are rewritten with finite series as [4]:

$$u_3 = \sum_{i=1} \phi_i(x_1) q_i(t) \tag{19}$$

$$\beta = \sum_{i=1} \psi_i(x_1) p_i(t) \tag{20}$$

where:

$$\phi_i(x_1) = \cos\beta_i x - \cosh\beta_i x - \frac{\cos\beta_i L + \cosh\beta_i L}{\sin\beta_i L + \sinh\beta_i L}(\sin\beta_i x - \sinh\beta_i x) \tag{21}$$

$$\psi_i(x_1) = -\sin\beta_i x - \sinh\beta_i x - \frac{\cos\beta_i L + \cosh\beta_i L}{\sin\beta_i L + \sinh\beta_i L}(\cos\beta_i x - \cosh\beta_i x) \tag{22}$$

where β is the solution of:

$$1 + \cos\beta L \cosh\beta L = 0 \tag{23}$$

2.4. Lagrange's equation and equations of motion

The Lagrange equation is:

$$\frac{d}{dt}\left(\frac{\partial T}{\partial \dot{q}_k}\right) - \frac{\partial T}{\partial q_k} + \frac{\partial U}{\partial q_k} - \frac{\partial W_e}{\partial q_k} = \frac{\partial W_{nc}}{\partial q_k}$$
$$q_k = \{q_1, q_2, \dots, q_n, p_1, p_2, \dots, p_n, v\} \tag{24}$$

The dimensionless parameters are defined as,

$$\xi = \frac{x_1}{L}, \bar{q} = \frac{q}{L}, \bar{v} = \frac{V}{V_0}, \bar{g} = \frac{g}{L}, \bar{L}_p = \frac{L_1}{L}, \tau = t\sqrt{\frac{EI_b}{\rho_b A_b L^4}}, \overline{\rho_p A_p} = \frac{\rho_p A_p}{\rho_b A_b}$$
$$\overline{\rho_p I_p} = \frac{\rho_p I_p}{\rho_b I_b}, \bar{C} = \frac{cL^5 A_b}{EI_b}\sqrt{\frac{EI_b}{\rho_b A_b L^4}} \tag{25}$$

$$I_b = A_b r_b^2, s_b^2 = \frac{L^2}{r_b^2}, \frac{A_p L^2}{I_b} = \frac{A_p L^2}{A_b r_b^2} = \bar{A}_p s_b^2, \bar{A}_p = \frac{A_p}{A_b}, \bar{I}_p = \frac{I_p}{I_b}, \bar{E}_p = \frac{c_{11}^{\epsilon}}{E}, \bar{G}_b = \frac{G_b}{E} \tag{26}$$

$$\bar{G}_p = \frac{c_{55}^{\epsilon}}{E}, C_p^S = 2e_{31}v_0\frac{Q_p}{h_p}\frac{L}{EI_b}, C_s^p = e_{31}\frac{1}{\xi_{33}^S A_e}\frac{Q_p}{V_0}, T = 2\frac{h_p}{\xi_{33}^S A_e R\sqrt{\frac{EI_b}{\rho_b A_b L^4}}} \tag{27}$$

The dimensionless dynamic equations of the system are:

$$\begin{aligned}
&\sum_{j=1}\frac{d^2\bar{q}_j}{d\tau^2}\left[\int_0^1\left(\frac{d\phi_i}{d\xi}\frac{d\phi_j}{d\xi}+s_b^2\phi_i\phi_j\right)d\xi+2\int_0^{\bar{L}_p}\left(\overline{\rho_p I_p}\frac{d\phi_i}{d\xi}\frac{d\phi_j}{d\xi}+s_b^2\overline{\rho_p A_p}\phi_i\phi_j\right)d\xi\right]\\
&-\sum_{r=1}\frac{d^2p_r}{d\tau^2}\left[\int_0^1\frac{d\phi_i}{d\xi}\psi_r d\xi+2\overline{\rho_p I_p}\int_0^{\bar{L}_p}\frac{d\phi_i}{d\xi}\psi_r d\xi\right]+\bar{C}\sum_{j=1}^{n}\frac{d^2\bar{q}_j}{d\tau^2}\phi_i\phi_j\delta(L_d)\\
&+\sum_{j=1}\bar{q}_j\left[s_b^2\int_0^1\frac{d^2\phi_i}{d\xi^2}\frac{d^2\phi_j}{d\xi^2}d\xi+2s_b^2\bar{E}_p\bar{I}_p\int_0^{\bar{L}_p}\frac{d^2\phi_i}{d\xi^2}\frac{d^2\phi_j}{d\xi^2}d\xi\right]\\
&+\sum_{j=1}\sum_{r=1}\sum_{s=1}\bar{q}_j\bar{q}_r\bar{q}_s\left[\frac{1}{2}s_b^4\int_0^1\frac{d\phi_i}{d\xi}\frac{d\phi_j}{d\xi}\frac{d\phi_r}{d\xi}\frac{d\phi_s}{d\xi}d\xi+s_b^4\bar{E}_p\bar{A}_p\int_0^{\bar{L}_p}\frac{d\phi_i}{d\xi}\frac{d\phi_j}{d\xi}\frac{d\phi_r}{d\xi}\frac{d\phi_s}{d\xi}d\xi\right]\\
&-s_b^2C_p^S\bar{v}\int_0^{\bar{L}_p}\frac{d^2\phi_i}{d\xi^2}d\xi=-\sum_{j=1}\frac{d^2\bar{g}}{d\tau^2}\left[s_b^2\int_0^1\phi_i d\xi+2s_b^2\overline{\rho_p A_p}\int_0^{\bar{L}_p}\phi_i d\xi\right]
\end{aligned} \tag{28}$$

$$\begin{aligned}
&-\sum_{j=1}\frac{d^2\bar{q}_j}{d\tau^2}\left(\int_0^1\psi_i\frac{d\phi_j}{d\xi}d\xi+2\overline{\rho_p I_p}\int_0^{\bar{L}_p}\psi_i\frac{d\phi_j}{d\xi}d\xi\right)\\
&+\sum_{r=1}\frac{d^2p_i}{d\tau^2}\left(\int_0^1\psi_i\psi_r d\xi+2\overline{\rho_p I_p}\int_0^{\bar{L}_p}\psi_i\psi_r d\xi\right)\\
&-\sum_{j=1}\bar{q}_j\left(s_b^2\int_0^1\frac{d\psi_i}{d\xi}\frac{d^2\phi_j}{d\xi^2}d\xi+2s_b^2\bar{E}_p\bar{I}_p\int_0^{\bar{L}_p}\frac{d\psi_i}{d\xi}\frac{d^2\phi_j}{d\xi^2}d\xi\right)\\
&+\sum_{r=1}p_r\left\{\int_0^1\left(s_b^2\frac{d\psi_i}{d\xi}\frac{d\psi_r}{d\xi}+\kappa s_b^4\bar{G}_b\psi_i\psi_r\right)d\xi+2\int_0^{\bar{L}_p}\left(s_b^2\bar{E}_p\bar{I}_p\frac{d\psi_i}{d\xi}\frac{d\psi_r}{d\xi}+\kappa s_b^4\bar{G}_p\bar{A}_p\psi_i\psi_r\right)d\xi\right\}\\
&+s_b^2C_p^S\bar{v}\int_0^{\bar{L}_p}\frac{d\psi_i}{d\xi}d\xi=0
\end{aligned} \tag{29}$$

$$\frac{d\bar{v}}{d\tau}+C_s^p\sum_{j=1}\frac{d\bar{q}_j}{d\tau}\left(\int_0^{\bar{L}_p}\frac{d^2\phi_1}{d\xi^2}d\xi\right)-C_s^p\sum_{r=1}\frac{dp_r}{d\tau}\left(\int_0^{\bar{L}_p}\frac{d\psi_r}{d\xi}d\xi\right)+T\bar{v}=0 \tag{30}$$

3. Complexifiaction averaging method

As it was mentioned before, the nonlinear equations must be solved analytically to achieve frequency response captures. For the uni-modal case, perturbation analysis is used in previous works but it is useless for the multimodal case. Complexification averaging method [11] is used in this paper for solving the equations (28-30). For showing the procedure of complex averaging method, we will solve the uni-modal case. The multimodal case has a similar procedure. Equations of motion in uni-modal case are:

$$m_{11}\ddot{\bar{q}}_1 + m_{12}\ddot{p}_1 + C_1\dot{\bar{q}}_1 + k_{11}\bar{q}_1 + k_{12}p_1 + K_{nl}\bar{q}_1^3 - \alpha\bar{v} = f\cos\Omega\tau \tag{31}$$

$$m_{12}\ddot{\bar{q}}_1 + m_{22}\ddot{p}_1 + k_{12}\bar{q}_1 + k_{22}p_1 + \beta\bar{v} = 0 \tag{32}$$

$$\dot{\bar{v}} + \lambda_1\dot{\bar{q}}_1 - \lambda_2\dot{p}_1 + T\bar{v} = 0 \tag{33}$$

For solving equations (31-33) new variables are defined as [4]:

$$\Psi_1 = \dot{\bar{q}}_1 + j\Omega\bar{q}_1\,, \qquad \Psi_2 = \dot{p}_1 + j\Omega p_1, \qquad \Psi_3 = \dot{\bar{v}} + j\Omega\bar{v}, \qquad j = \sqrt{-1} \tag{34}$$

As a result:

$$\begin{gathered}\bar{q}_1 = \frac{\Psi_1 - \Psi_1^*}{2j\Omega}, \dot{\bar{q}}_1 = \frac{\Psi_1 + \Psi_1^*}{2}, \ddot{\bar{q}}_1 = \dot{\Psi}_1 - j\Omega\frac{\Psi_1 + \Psi_1^*}{2}, p_1 = \frac{\Psi_2 - \Psi_2^*}{2j\Omega}, \dot{p}_1 = \frac{\Psi_2 + \Psi_2^*}{2} \\ \ddot{p}_1 = \Psi_2 - j\Omega\frac{\Psi_2 + \Psi_2^*}{2}, \bar{v} = \frac{\Psi_3 - \Psi_3^*}{2j\Omega}, \dot{\bar{v}} = \frac{\Psi_3 + \Psi_3^*}{2}\end{gathered} \tag{35}$$

where $*$ shows the complex conjugate of the variable. Solutions of Ψ_1, Ψ_2 and Ψ_3 in the complex averaging method is considered a harmonic with the same frequency of actuation as:

$$\begin{gathered}\Psi_1(\tau) = \Phi_1(\tau)e^{j\Omega\tau}, \Psi_1^*(\tau) = \Phi_1^*(\tau)e^{-j\Omega\tau}, \Psi_2(\tau) = \Phi_2(\tau)e^{j\Omega\tau}, \\ \Psi_2^*(\tau) = \Phi_2^*(\tau)e^{-j\Omega\tau}, \Psi_3(\tau) = \Phi_3(\tau)e^{j\Omega\tau}, \Psi_3^*(\tau) = \Phi_3^*(\tau)e^{-j\Omega\tau}\end{gathered} \tag{36}$$

Substituting (36) into (35) and substituting the result in equations (31-33) and considering only the slow terms leads to:

$$m_{11}\left(\dot{\Phi}_1 + \frac{j\Omega\Phi_1}{2}\right) + m_{12}\left(\dot{\Phi}_2 + \frac{j\Omega\Phi_2}{2}\right) + \frac{C_1}{2}\Phi_1 - k_{11}\frac{j\Phi_1}{2\Omega} - k_{12}\frac{j\Phi_2}{2\Omega} - 3k_{nl}\frac{j\Phi_1^*\Phi_1^2}{8\Omega^3} + \alpha\frac{j\Phi_3}{2\Omega} = \frac{f}{2} \tag{37}$$

$$m_{12}\left(\dot{\Phi}_1 + \frac{j\Omega\Phi_1}{2}\right) + m_{22}\left(\dot{\Phi}_2 + \frac{j\Omega\Phi_2}{2}\right) - k_{12}\frac{j\Phi_1}{2\Omega} - k_{22}\frac{j\Phi_2}{2\Omega} - \beta\frac{j\Phi_3}{2\Omega} = 0 \tag{38}$$

$$\Phi_3 + \lambda_1\Phi_1 - \lambda_2\Phi_2 - T\frac{j\Phi_3}{2\Omega} = 0 \tag{39}$$

For steady state condition, equations (37-39) lead to algebraic equations that can be solved easily and solving them results in the limit cycle oscillations of primary system. Multimodal equations of motion can be solved with a similar procedure.

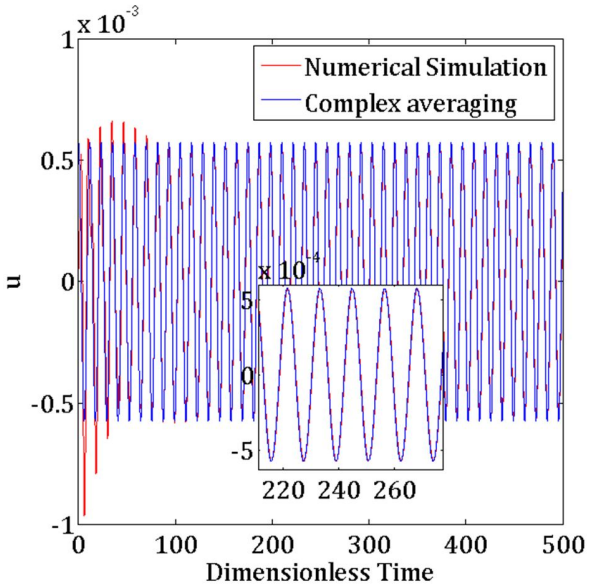

Fig. 2. Validation of the result of complex averaging method

4. Results and discussion

In order to validate the response of the system, a numerical simulation using the Runge-Kutta method is compared with the response achieved by complexification averaging method. Fig. 2 shows the high accuracy of the method in steady-state response of the system. Solving the algebraic equations achieved from the complex averaging method leads to the amplitude of the limit cycle oscillations. Therefor, for frequency response captures, these algebraic equations should be solved for a range of frequencies but this work could be impossible or time consuming for some frequencies. Hence, the Arc-length Continuation method is used. Values of geometric and material properties of the system are showed in the Table 1 [12].

Table 1. Geometric and material properties

Name	Symbol	Value
Beam thickness	h_b	$0.2e-3\ (m)$
Piezoelectric layer thickness	h_p	$0.2e-3(m)$
Beam and piezoelectric width	w_b	$25.4e-3\ (m)$
Beam length	L	$200e-3\ (m)$
Piezoelectric layer length	L_p	$80e-3\ (m)$
Young's modulus of Beam	E	$70e9\ (pa)$
Young's modulus of piezoelectric layer	c_{11}^{ϵ}	$60e9\ (pa)$
Shear modulus of beam	G	$26.9e9\ (pa)$
Shear modulus of piezoelectric layer	c_{55}^{ϵ}	$25.2e9\ (pa)$
Shear stress correction coefficient	k	$5/6$
Resistance of resistive load	R	$4.5e5\ (\Omega)$
Piezoelectric permittivity constant of	ξ_{33}^{S}	$25.55e-9\ (F/m)$
Effective piezoelectric constant	e_{31}	$-16.6\ (C/m)$

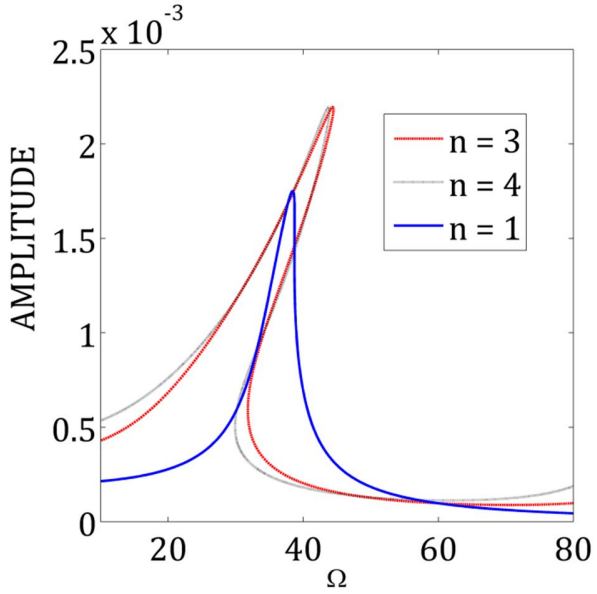

Fig. 3. Effect of number of shape modes on amplitude of vibration

Fig. 3 shows that the solution is converged in more than two mode shapes. Fig. 4 shows that the uni-modal case can't predict the second, third and higher resonance peaks of the response. In the uni-modal case, there is a region that three different amplitudes are available. However, in the multimodal case, there is a region that five different amplitudes are available. Fig. 5 shows the stability analysis of the frequency response of the system. It indicates that the response of medium range amplitude is unstable and the two others are stable.

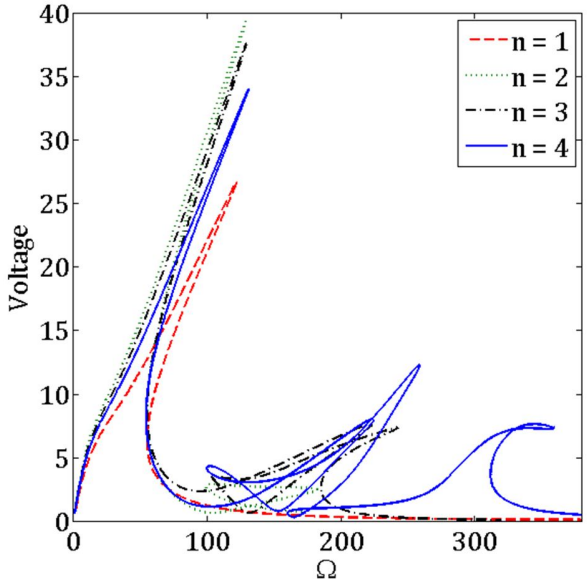

Fig. 4. Effect of number of shape modes on output voltage

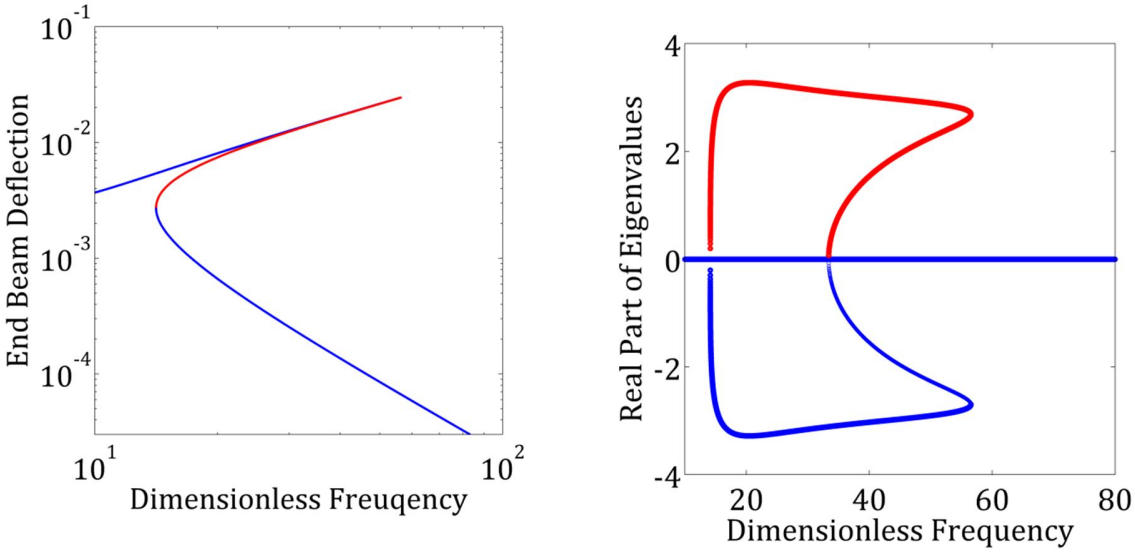

Fig. 5. Stability analysis of the frequency response

As it can be seen in Fig. 6, increase in the length of the beam results in increase of output voltage and decrease in vibration amplitude . It is an obvious result because the rate of strain is more in the root of the beam. Fig. 7 shows that in higher base acceleration, both end deflection vibration and output voltage are higher because more energy is applied to the base of the system.

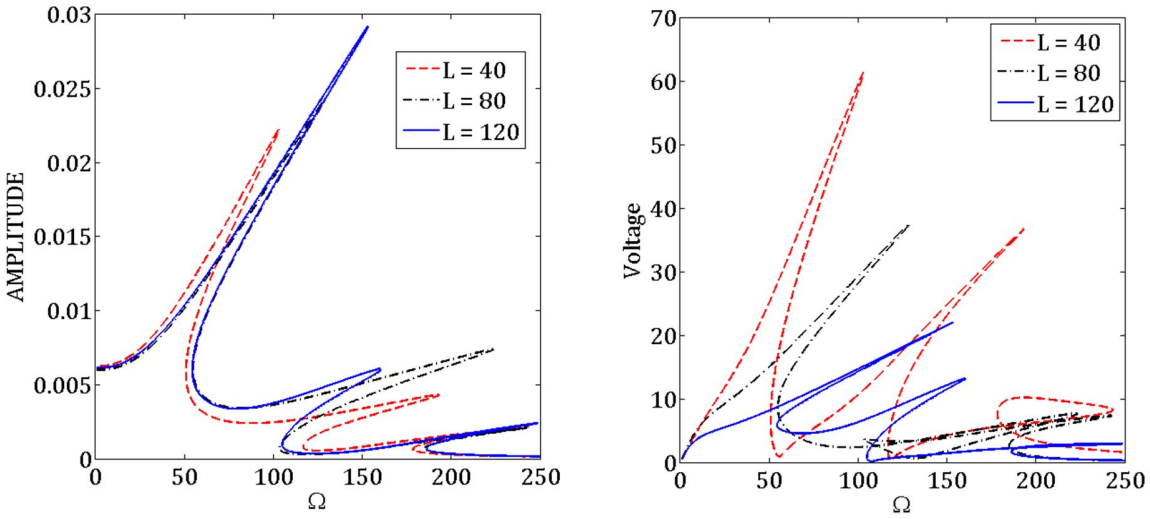

Fig. 6. Effect of piezoelectric layers length on the amplitude of end deflection and output voltage

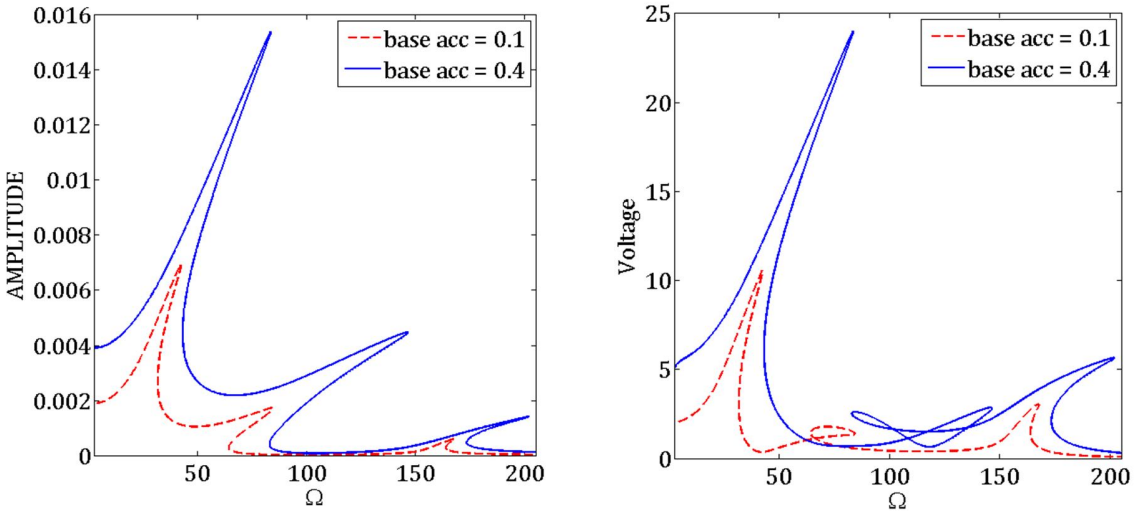

Fig. 7. Effect of base acceleration on the amplitude of end deflection and output voltage

5. Conclusion

A cantilever beam is modeled as a Timoshenko beam using Assumed Mode Method in this paper. The derived equations of motion are solved using the Complex Averaging Method. Frequency response captures are achieved using the Arc-length Continuation method. Frequency captures are provided for different values of problem parameters and it is understood that:

1. Unimodal consideration can't predict the behavior of the system correctly and the solution is converged in more than two mode shapes of vibration.

2. Increasing base acceleration results in increasing amplitude of vibration and output voltage.

3. Power generation is maximum when the ends of the piezoelectric layers are close to the root of the beam.

References

[1] S.R. Anton, H.A. Sodano, A review of power harvesting using piezoelectric materials (2003–2006), Smart Materials and Structures, 16 (2007) R1.
[2] V.R. Challa, M.G. Prasad, Y. Shi, F.T. Fisher, A vibration energy harvesting device with bidirectional resonance frequency tunability, Smart Materials and Structures, 17 (2008) 015035.
[3] M.F. Daqaq, R. Masana, A. Erturk, D.D. Quinn, On the role of nonlinearities in vibratory energy harvesting: a critical review and discussion, Applied Mechanics Reviews, 66 (2014) 040801.
[4] B.P. Mann, N.D. Sims, Energy harvesting from the nonlinear oscillations of magnetic levitation, Journal of Sound and Vibration, 319 (2009) 515-530.
[5] G. Sebald, H. Kuwano, D. Guyomar, B. Ducharne, Experimental Duffing oscillator for broadband piezoelectric energy harvesting, Smart materials and structures, 20 (2011) 102001.
[6] G. Sebald, H. Kuwano, D. Guyomar, B. Ducharne, Simulation of a Duffing oscillator for broadband piezoelectric energy harvesting, Smart Materials and Structures, 20 (2011) 075022.

[7] M.A. Karami, D.J. Inman, Equivalent damping and frequency change for linear and nonlinear hybrid vibrational energy harvesting systems, Journal of Sound and Vibration, 330 (2011) 5583-5597.
[8] M.F. Daqaq, Response of uni-modal duffing-type harvesters to random forced excitations, Journal of Sound and Vibration, 329 (2010) 3621-3631.
[9] W.A. Jiang, L.Q. Chen, Energy harvesting of monostable Duffing oscillator under Gaussian white noise excitation, Mechanics Research Communications, 53 (2013) 85-91.
[10] R. Masana, M.F. Daqaq, Response of duffing-type harvesters to band-limited noise, Journal of Sound and Vibration, 332 (2013) 6755-6767.
[11] A.F. Vakakis, O.V. Gendelman, L.A. Bergman, D.M. McFarland, G. Kerschen, Y.S. Lee, Nonlinear targeted energy transfer in mechanical and structural systems, Springer Science & Business Media, 2008.
[12] A. Erturk, Assumed-modes modeling of piezoelectric energy harvesters: Euler–Bernoulli, Rayleigh, and Timoshenko models with axial deformations, Computers & Structures, 106 (2012) 214-227.